Published in final edited form as:
Bone. 2014 September ; 66: 277–286. doi:10.1016/j.bone.2014.06.022.

Runx2 is required for early stages of endochondral bone formation but delays final stages of bone repair in Axin2-deficient mice

Meghan E. McGee-Lawrence[1], **Lomeli R. Carpio**[1], **Elizabeth W. Bradley**[1], **Amel Dudakovic**[1], **Jane B. Lian**[2], **Andre J. van Wijnen**[1], **Sanjeev Kakar**[1], **Wei Hsu**[3], and **Jennifer J. Westendorf**[1]

[1]Mayo Clinic, Rochester, MN USA

[2]University of Vermont, Burlington VT USA

[3]University of Rochester Medical Center, Rochester, NY USA

Abstract

Runx2 and Axin2 regulate skeletal development. We recently determined that Axin2 and Runx2 molecularly interact in differentiating osteoblasts to regulate intramembranous bone formation, but the relationship between these factors in endochondral bone formation was unresolved. To address this, we examined the effects of Axin2 deficiency on the cleidocranial dysplasia (CCD) phenotype of *Runx2*$^{+/-}$ mice, focusing on skeletal defects attributed to improper endochondral bone formation. Axin2 deficiency unexpectedly exacerbated calvarial components of the CCD phenotype in the *Runx2*$^{+/-}$ mice; the endocranial layer of the frontal suture, which develops by endochondral bone formation, failed to mineralize in the *Axin2*$^{-/-}$*:Runx2*$^{+/-}$ mice, resulting in a cartilaginous, fibrotic and larger fontanel than observed in *Runx2*$^{+/-}$ mice. Transcripts associated with cartilage development (e.g., Acan, miR140) were expressed at higher levels, whereas blood vessel morphogenesis transcripts (e.g., Slit2) were suppressed in *Axin2*$^{-/-}$*:Runx2*$^{+/-}$ calvaria. Cartilage maturation was impaired, as primary chondrocytes from double mutant mice demonstrated delayed differentiation and produced less calcified matrix in vitro. The genetic dominance of Runx2 was also reflected during endochondral fracture repair, as both *Runx2*$^{+/-}$ and double mutant *Axin2*$^{-/-}$*:Runx2*$^{+/-}$ mice had enlarged fracture calluses at early stages of healing. However, by the end stages of fracture healing, double mutant animals diverged from the *Runx2*$^{+/-}$ mice, showing smaller calluses and increased torsional strength indicative of more rapid end stage bone formation as seen in the *Axin2*$^{-/-}$ mice. Taken together, our data demonstrate a

Corresponding author: Jennifer J. Westendorf, Ph.D., Mayo Clinic, 200 First Street SW, Rochester, MN 55905, Phone: 507-538-5651 / Fax: 507-284-5075, westendorf.jennifer@mayo.edu.

Disclosure
All authors have no conflicts of interest.

dominant role for Runx2 in chondrocyte maturation, but implicate Axin2 as an important modulator of the terminal stages of endochondral bone formation.

Keywords

cleidocranial dysplasia; Runx2; Axin2; Wnt signaling; endochondral bone formation

1. Introduction

The crucial roles of the skeleton include being a mineral reservoir, providing a structural frame for soft tissues to facilitate locomotion, and protecting internal organs. Improper bone formation negatively impacts organism development and function. In particular, premature fusion of any of the cranial sutures (craniosynostosis), which appears in 1 of 2,500 live births [1], may cause cognitive delays and disfigurement if corrective surgery is not performed. Another genetic birth defect, cleidocranial dysplasia, impairs the formation of cranial vault and other bones, placing the brain at risk for damage and limiting both skeletal size and strength [2, 3].

Bones develop and repair by two mechanisms: intramembranous and endochondral ossification [4]. During intramembranous bone formation, mesenchymal progenitor cells condense and directly differentiate into osteoblasts. This occurs during formation of the lateral aspects of the clavicle and many skull bones, as well as during the repair of fully stabilized fractures (e.g., distraction osteogenesis) [5, 6]. In contrast, during endochondral ossification, mesenchymal progenitor cells first form a cartilaginous anlage that becomes vascularized to recruit osteoblast precursors. Endochondral ossification promotes long bone development, the repair of unstable fractures (via callus formation), the fusion of some cranial sutures, and development of the medial clavicle [7-9]. Both intramembranous and endochondral ossification processes utilize many of the same molecules, including the master osteoblast transcription factor Runx2 and components of the Wnt signaling pathway.

Although much is known about how Runx2 interfaces with the Wnt signaling pathway in vitro, less is known about how they interact during skeletal development and repair in vivo. Runx2 is essential for proper skeletal morphogenesis and maintenance because it contributes to both intramembranous and endochondral bone formation processes. Germline deletion of Runx2 is lethal because it prevents formation of a mature, mineralized skeleton [3, 10]. This phenotype is recapitulated in mice where Runx2 is only ablated in chondrocytes but not in mice lacking Runx2 in committed osteoblasts [11]. Thus, Runx2 is required for osteoblastogenesis and terminal chondrocyte maturation. Haploinsufficiency in Runx2 causes cleidocranial dysplasia (CCD), a genetic disorder characterized by developmental skeletal defects including impaired closure of cranial sutures, persistent fontanels in the calvaria, supernumerary teeth, and hypoplastic or absent clavicles [3, 12]. Although CCD is most often associated with deficiencies in intramembranous bone formation, endochondral bone formation is also negatively impacted [9, 11, 13]. Overexpression of Runx2 in the condensing skeletal mesenchyme may produce an opposing craniofacial deformation as RUNX2 duplication was found in a human case of metopic craniosynostosis [14], and

Runx2 transgenic mice develop craniosynostosis and ectopic bone formation due to improper differentiation of Prx1-positive progenitor cells to the osteoblastic lineage [15]. Proper Wnt signaling is also essential for proper skeletal development, particularly in craniofacial locations. Axin2, a downstream target and negative feedback inhibitor of canonical Wnt signaling, is expressed in the developing sutures of the mouse skull [16, 17]. Axin2-deficient mice develop craniosynostosis with rapid closure of the cranial sutures as early as postnatal day 7 [16, 17], which phenotypically opposes the delayed suture closure and persistent fontanels in the Runx2$^{+/-}$ mice. Craniosynostosis in *Axin2*$^{-/-}$ mice is directly attributed to enhanced β-catenin-dependent Wnt signaling because nuclear β-catenin levels are high in *Axin2*$^{-/-}$ osteoprogenitor cells and *Ctnnb* haploinsufficiency prevents craniosynostosis in *Axin2*$^{-/-}$ mice [16].

We recently discovered that Axin2 and Runx2 molecularly interact in osteoblasts [18], and that this interaction controls intramembranous bone formation mechanisms in vivo. Given the phenotypically opposing craniofacial phenotypes of *Runx2*$^{+/-}$ and *Axin2*$^{-/-}$ mice, we sought to determine whether Axin2 and Runx2 are part of the same molecular pathway that regulates endochondral bone formation in vivo by investigating developmental and regenerative aspects of skeletal morphogenesis in wildtype (WT), *Axin2*$^{-/-}$, *Runx2*$^{+/-}$, and double mutant *Axin2*$^{-/-}$*: Runx2*$^{+/-}$ mice. Strikingly, Axin2 deficiency did not rescue, but instead exacerbated the CCD phenotype in *Runx2*$^{+/-}$ mice. This was associated with increased cartilage in the frontal suture, which naturally fuses by endochondral mechanisms. Additional models, including in vitro chondrocyte cultures and transverse endochondral fracture healing, confirmed that Runx2 is required for endochondral bone formation in the presence or absence of Axin2 deficiency.

2. Materials & Methods

2.1 Animal studies

All animal research was conducted according to guidelines provided by the National Institutes of Health and the Institute of Laboratory Animal Resources, National Research Council. The Mayo Clinic Institutional Animal Care and Use Committee approved all animal studies. *Runx2*$^{+/-}$ mice [16, 17, 19] on a mixed BDF1 and B6 background were crossed with *Axin2*$^{+/-}$ and *Axin2*$^{-/-}$ mice [17] on a mixed 129 and B6 background to generate double mutant *Axin2*$^{-/-}$*: Runx2*$^{+/-}$ mice along with wildtype (WT) and single mutant *Runx2*$^{+/-}$ or *Axin2*$^{-/-}$ littermates. Genotypes were determined as previously described [18]. Animals were housed in an accredited facility under a 12-hour light/dark cycle and provided water and food (PicoLab Rodent Diet 20, LabDiet) ad libitum. All studies were conducted with male mice.

2.2 Whole mount staining

Skeletons from 1 week-old mouse pups were dissected and fixed overnight in ethanol. Cartilage elements were stained with a 30% Alcian blue dye (dissolved in 80 ml 95% ethanol and 20 ml glacial acetic acid). Skeletons were washed twice with 95% ethanol and then placed in 2% KOH until the remaining soft tissues were dissolved. Bones were stained with 75 μg/ml Alizarin red S (Sigma) in 1% KOH overnight and then destained in 20%

glycerol, 1% KOH for 2 weeks, with daily solution changes. Skeletons were transferred to a 20% glycerol, 20% ethanol solution overnight and then stored in a 50% glycerol, 50% ethanol solution.

2.3 Analysis of CCD phenotype: clavicle and cranial fontanel morphology

Clavicle morphology was quantified via digital X-ray (Faxitron LX-60) and image analysis software (Bioquant Osteo, Nashville TN) in 1-, 4-, and 24 week-old mice. Projected clavicle area and width were quantified for both right and left clavicles and averaged for each mouse. Cranial fontanel morphology was assessed via micro-computed tomography (microCT) at 4 and 24 weeks of age. Skulls were scanned in 70% ethanol on a μCT35 scanner (Scanco Medical AG, Basserdorf, Switzerland) at 20 μm (4 week-old animals) or 30 μm (24 week-old animals) resolution (energy settings: 70 kV, 114 μA; integration time: 300 ms) and reconstructed with the manufacturer's software using a threshold value of 150. The area of the fontanel defect was quantified from dorsal views using image analysis software (Bioquant Osteo).

2.4 RNA extraction

Calvaria containing parietal and frontal bones from 1 week-old pups were dissected from soft tissues, rinsed with HBSS, and digested in collagenase digestion medium [20] on an orbital shaker for 20 minutes at 37° C and 125 rpm. Following digestion, explants were washed once with PBS and snap frozen in liquid nitrogen [21]. Explants were homogenized in TRIzol reagent (Invitrogen) using a high-speed disperser (Ultra-Turrax T25, IKA) and RNA was extracted and purified from the ground tissue according to the TRIzol manufacturer's protocol, which included an overnight incubation at −20° C in 100% isopropanol to facilitate precipitation of microRNA (miR) and messenger RNA (mRNA).

2.5 Microarray analysis of calvarial mRNA expression

For microarray analysis of gene expression, RNA was reverse transcribed using Qiagen's Quantitect Reverse Transcription Kit and transcript levels were determined with the Illumina MouseRef-8 BeadChip array. Four mice from each genotype (WT, *Runx2*$^{+/-}$, *Axin2*$^{-/-}$, and *Axin2*$^{-/-}$*:Runx2*$^{+/-}$) were analyzed. One *Axin2*$^{-/-}$ sample was lost from the BeadChip array during processing due to a technical error. Raw data were pre-processed using Beadstudio (Illumina Inc, San Diego, CA) and submitted to the MIAME-compliant GEO database (Accession number: **in progress**). Genes that were not expressed (detection $p \geq 0.05$) were eliminated from analysis, leaving 11,153 gene transcripts out of 18,138 for the final analysis. A paired t-test was used to compare differential gene expression between each mutant and WT mice, but pairwise comparisons were not made directly between each mutant group. Genes with fold changes greater than 1 standard deviation ($p < 0.05$) were used for pathway analysis of process networks using MetaCore software (GeneGo Inc, St. Joseph, MI, USA). Selected genes were subjected to reverse transcription (RT) and real-time semi-quantitative PCR (qPCR) analysis for confirmation as previously described [21]. RT was performed using the SuperScript III First-Strand Synthesis System (Invitrogen), and PCRs were performed using 37.5 ng of cDNA per 15 μl with Bio-Rad iQ SYBR Green Supermix and the Bio-Rad MyiQ Single Color Real-Time PCR Detection System. Transcript levels were

normalized to the reference gene Gapdh. Quantification was done using the $2^{-\Delta\Delta Ct}$ method [22]. Gene specific primers sequences are presented in Supplemental Table 1.

2.6 Microarray analysis of calvarial microRNA expression

Microarray analysis of miR expression was performed using the Affymetrix GeneChip miRNA Array. Raw data were pre-processed with Partek "microRNA Expression" workflow (Partek Incorporated, St. Louis, MO). Hierarchical clustering revealed that one *Runx2*$^{+/-}$ sample was an outlier; it was excluded from later analyses. MicroRNAs that were not expressed (detection $p \geq 0.05$) were eliminated from analysis, leaving 1125 out of 7815 for the final analysis.

2.7 Immunohistochemical and histological analysis of the frontal suture

Skulls from eight-day old mice were incubated for seven days in 15% EDTA; decalcification was confirmed by X-ray. Decalcified skulls were embedded in paraffin and sectioned longitudinally through the frontal suture at a thickness of 8 microns. Immunohistochemical staining was performed with monoclonal antibodies directed to active β-catenin that is un-phosphorylated on Ser33/37 and Thr41 (D13A1, Cell Signaling #8814, 1:50 dilution) or an IgG isotype control (Vector Laboratories I-1000). Specimens were incubated with polyvalent secondary HRP-conjugated antibodies (Abcam ab93697), followed by 3′-3′-diaminobenzidine (DAB) (Sigma Aldrich), and then counterstained with fast green. Skulls from 4 week-old mice were histologically processed and embedded in glycolmethacrylate. MicroCT scans of the embedded skulls were used to locate the frontal suture, which closes prematurely in Axin2$^{-/-}$ mice [17]. Thin (5 μm) sections were mounted and stained with Safranin O/Light Green. Cell and bone morphology were examined at 100× and 400× magnification.

2.8 Isolation and culture of immature mouse articular chondrocytes (IMACs)

Immature mouse articular chondrocytes (IMACs) were isolated and cultured in micromass as previously described [23, 24]. Chondrocytes in this model proceed through a defined differentiation program, expressing angiogenic factors like Vegf, matrix metalloproteinases such as Mmp13, and producing a proteoglycan-rich matrix that is calcified at 21 days in culture. Briefly, the femoral head and tibial plateau were dissected from 4 week-old mice. Cartilage pieces were digested twice in 3 mg/ml collagenase for one hour and then overnight in 0.5 mg/ml collagenase. The resulting IMACs were placed in micromass culture by plating 10 μl drops containing 2×10^5 cells in DMEM, 5% FBS supplemented with 25 μg/ml ascorbic acid, 54 μg/ml β-glycerol phosphate and 1× ITS (Invitrogen, Carlsbad, CA) as previously published [25-27]. Culture medium was changed every three days for 21 days. Cells were fixed after 21 days in culture and stained with either Alcian blue (to highlight matrix proteoglycan content) or Alizarin red (to highlight matrix calcification). For gene expression studies, RNA was harvested with TRIzol reagent (Invitrogen) after 21 days in culture. RNA was reverse transcribed and expression levels of genes associated with chondrocyte maturation were quantified as described above and previously [28]. Gene specific primer sequences are listed in Supplemental Table 1.

2.9 Quantification of femur length and trabecular bone mass in the distal femoral metaphysis

One femur from each of the 4- and 24-week old mice was cleaned of soft tissue, fixed in 10% neutral buffered formalin, and stored in 70% ethanol. Femur length was quantified as the distance from the top of the femoral head to the bottom of the medial condyle. Trabecular bone in the distal metaphysis of each femur was scanned in 70% ethanol on a μCT35 scanner (Scanco Medical AG, Basserdorf, Switzerland) at 7 μm voxel size using the energy settings described above. A region of interest was analyzed in each mouse, ranging from 6% to 13% of bone length (as measured proximally from the distal femoral growth plate) in 4-week old animals and from 14% to 19% of bone length (as measured proximally from the distal femoral epiphysis) in 24-week old animals. Trabecular bone volume fraction (Tb. BV/TV, %), trabecular number (Tb.N, mm^{-1}), trabecular thickness (Tb.Th, mm), and trabecular separation (Tb.Sp, mm), were computed using the manufacturer's software.

2.10 Endochondral fracture repair model

Closed fractures were created in the right femur as described previously [8, 29]. Buprenorphine was provided perioperatively at 0.09 mg/kg and acetaminophen was administered in drinking water (1 mg/mL) 24 hours before the surgery and continued until the animals were sacrificed. Mice were anesthetized with isoflurane during the procedure. Intramedullary fixation was carried out using the trochar of a 25G spinal needle inserted into the femoral medullary canal, after which mice were subjected to the creation of a closed femoral fracture using an Einhorn fracture device [8]. Mice were anesthetized with isoflurane for longitudinal monitoring via X-ray on days 7, 14, 21, and 28 post-fracture. Projected radiographical callus area was quantified with image analysis software (Bioquant Osteo) from these X-rays to assess the degree of callus formation and the rate of callus remodeling. Mice were sacrificed 21 days after fracture for histological and microCT analysis of the healing femurs or 30 days after fracture for torsional analysis of bone mechanical strength.

For morphological analysis, bones were fixed in 10% neutral buffered formalin and scanned in 70% ethanol on a μCT35 scanner (Scanco) at 20 μm resolution using the energy settings described above. Scans were reconstructed with the manufacturer's software using a threshold value of 150. After scanning, femurs were embedded in glycolmethacrylate, and thin (5 μm) sections were mounted and stained with Safranin O/Light Green protocol to highlight bone, cartilage, and connective tissues.

To quantify torsional strength, fractured femurs were harvested, cleaned of soft tissues, wrapped in saline soaked gauze, and stored at −20° C to preserve mechanical properties. The proximal and distal ends of each femur were potted in ¼ inch square brass endcaps (aligned with a custom jig) using cyanoacrylate and an accelerant (ZipKicker CA accelerator, Robart Manufacturing) to promote rapid bulk curing. On the day of testing, bones were thawed in 0.9% saline for at least one hour prior to testing, then loaded to failure at an actuator head displacement rate of 1 degree per second on a custom torsion testing apparatus featuring a 100 oz-inch torque cell (Transducer Techniques RTS 100). Ultimate torque and torsional rigidity were calculated from the load-deformation curves.

2.11 Statistics

Statistics were performed with JMP 9.0 statistical analysis software (SAS Institute Inc., Cary, NC). Data were compared between groups within each experiment with Student's t-tests or ANOVA with post-hoc comparisons. A significance of $p < 0.05$ was used for all comparisons.

3. Results

3.1 Loss of Axin2 exacerbates the Runx2$^{+/-}$ mouse CCD phenotype

The CCD phenotype of *Runx2*$^{+/-}$ mice is characterized by hypoplastic clavicles and persistent calvarial fontanels. Since Axin2 deficiency promotes bone formation through increased Wnt signaling, we generated double mutant *Axin2*$^{-/-}$*:Runx2*$^{+/-}$ animals to determine if Axin2-deficiency would rescue the CCD phenotype. As expected, clavicles were severely hypoplastic in *Runx2*$^{+/-}$ mice as compared to WT mice, demonstrating a 70% reduction in projected clavicle area and a 25% decrease in average width compared to WT mice at 1 week of age (Figure 1A-C). These differences remained in the *Runx2*$^{+/-}$ animals at 4 and 24 weeks of age. Introducing Axin2 deficiency into this model did not rescue clavicle morphogenesis, as clavicle area and width were 73% and 40% smaller, respectively, in *Axin2*$^{-/-}$:*Runx2*$^{+/-}$ mice as compared to WT animals at 1 week of age (Figure 1A-C). Deficiencies in clavicle development were most commonly noted in the medial aspect of the clavicle, which develops by endochondral, rather than intramembranous, bone formation [9] (Figure 1A; note arrow). Clavicles remained smaller in *Axin2*$^{-/-}$*:Runx2*$^{+/-}$ mice as compared to WT mice at 4- and 24-weeks of age, but were statistically comparable to *Runx2*$^{+/-}$ littermates. Clavicle morphology was comparable between *Axin2*$^{-/-}$ and WT mice at all ages investigated (Figure 1A-C).

Whole mount staining revealed delayed skull development and a distinct fontanel in the calvaria of *Runx2*$^{+/-}$ mice but not in WT or *Axin2*$^{-/-}$ mice at 1 week of age. Calvarial development was further impaired in the *Axin2*$^{-/-}$*:Runx2*$^{+/-}$ animals, and by 4 weeks of age, this fontanel was 125% larger in *Axin2*$^{-/-}$*:Runx2*$^{+/-}$ animals as compared to *Runx2*$^{+/-}$ littermates (Figure 2). By 24 weeks of age, fontanel size was 225% greater in *Axin2*$^{-/-}$*:Runx2*$^{+/-}$ mice (Figure 2). Thus, Axin2 deficiency did not rescue, but instead exacerbated the calvarial phenotype of the *Runx2*$^{+/-}$ animals.

3.2 Cartilage persists in the frontal suture of Axin2$^{-/-}$:Runx2$^{+/-}$ mice

Closer examination of the skull microCT reconstructions from 4 week- and 24 week-old animals revealed that the enlarged fontanel in the *Axin2*$^{-/-}$*:Runx2*$^{+/-}$ mice originated within the frontal suture. The murine frontal suture features a bilayer of ecto- and endocranial tissue and fuses under normal developmental conditions by endochondral, rather than intramembranous, bone formation [30, 31]. Fusion begins in the most anterior aspect of the suture, and is completed by 39 to 45 days after birth [30]. Digital sectioning through microCT reconstructions from 4 week-old skulls revealed a normal, bilayer frontal suture development in WT mice that was not yet fully fused at postnatal day 28 (Figure 3). Similar morphology was present in the *Runx2*$^{+/-}$ animals, although the fusion was delayed, evidenced by a larger gap between the frontal bones of *Runx2*$^{+/-}$ mice compared to WT

littermates. In contrast, as previously reported [16, 17], the frontal suture of *Axin2*$^{-/-}$ mice was completely fused at 4 weeks of age. Interestingly, the frontal suture failed to properly develop in the *Axin2*$^{-/-}$*:Runx2*$^{+/-}$ animals as there was no visible mineralization of the endocranial layer by microCT (Figure 3). Safranin O staining of the frontal suture of 4 week-old animals confirmed the presence of cartilage and absence of mature, mineralized tissue in the frontal suture of the *Axin2*$^{-/-}$*:Runx2*$^{+/-}$ animals at 4 weeks of age (Figure 4). Low levels of active, nuclear β-catenin were detected in the endocranial layer of the frontal suture of 8 day-old *Runx2*$^{+/-}$ and *Axin2*$^{-/-}$*:Runx2*$^{+/-}$ mice (Figure 5). In contrast, the endocranial layer of the frontal suture in WT and *Axin2*$^{-/-}$ mice showed considerable maturation (via fast green staining of bone tissue) and nuclear β-catenin staining (Figure 5).

3.3 Gene expression patterns reflect improper endochondral bone formation in the calvaria of Axin2$^{-/-}$: Runx2$^{+/-}$ mice

Calvarial mRNA and microRNA arrays were performed to uncover developmental and signaling pathways contributing to the large fontanel development in *Axin2*$^{-/-}$ *:Runx2*$^{+/-}$ animals. Compared to WT littermates, *Axin2*$^{-/-}$*:Runx2*$^{+/-}$ mice differentially expressed 902 genes. Nearly half (n=491) of these genes were unique to the *Axin2*$^{-/-}$*:Runx2*$^{+/-}$ mice and were not changed in calvaria from either single mutant animal as compared to WT mice (Figure 6A). Process network analysis of these 491 genes in Metacore identified two key pathways, blood vessel morphogenesis and cartilage development, which were affected in the *Axin2*$^{-/-}$*:Runx2*$^{+/-}$ mice (Figure 6B). Transcripts associated with cartilage development were increased (Figure 6C), but transcripts for blood vessel morphogenesis factors were decreased the *Axin2*$^{-/-}$ *:Runx2*$^{+/-}$ animals (Figure 6D). These patterns are consistent with the presence of cartilage in the frontal suture of double mutant mice observed histologically at 4 weeks of age. *Runx2*$^{+/-}$ mice differentially expressed 597 genes (302 unique) and *Axin2*$^{-/-}$ mice differentially expressed 835 genes (590 unique) as compared to WT littermates (Figure 6A). Process network analysis failed to identify significantly affected pathways exclusive to the *Runx2*$^{+/-}$ mice, but identified Wnt signaling as being the primary pathway uniquely activated in *Axin2*$^{-/-}$ animals (Figure 6B).

Axin2$^{-/-}$*:Runx2*$^{+/-}$ mice differentially expressed 41 miRs as compared to WT littermates; 38 of these were unique to the double mutants as compared to either single mutant animal. The most highly induced, unique miR in these animals was miR124, which was expressed 3.3 fold higher in *Axin2*$^{-/-}$*:Runx2*$^{+/-}$ mice as compared to WT animals. Other induced miRs in the double mutant animals were miR134, miR140, and miR455*. *Runx2*$^{+/-}$ mice differentially expressed 15 miRs (9 unique) and *Axin2*$^{-/-}$ mice differentially expressed 13 miRs (8 unique) (Figure 6A).

3.4 Primary chondrocytes from Axin2$^{-/-}$:Runx2$^{+/-}$ mice demonstrate delayed maturation

To determine if the unique developmental patterns seen in the skull could be recapitulated in a cell autonomous manner using in vitro models, primary immature articular chondrocytes (IMACs) were isolated from 4 week-old WT, *Runx2*$^{+/-}$, *Axin2*$^{-/-}$, and double mutant animals (Figure 7A). Chondrocytes derived from *Axin2*$^{-/-}$*:Runx2*$^{+/-}$ animals showed deficiencies in both proteoglycan deposition (by Alcian Blue staining) and matrix mineralization (by Alizarin Red staining) (Figure 7A) after 21 days in culture. Analysis of

mRNA expression revealed that these cells expressed high levels of aggrecan (Acan), but low levels of genes expressed by mature chondrocytes including osteopontin and Mepe (Figure 7B-D), suggesting delayed maturation. No differences were seen in expression of chondrocyte-specific transcription factors, including Sox5 and Sox9 (data not shown).

3.5 Trabecular bone mass is not affected in double mutant mice

Femoral length and trabecular bone mass were quantified in 4- and 24-week old male animals to determine if endochondral bone formation was dysregulated during long bone development of *Axin2−/−:Runx2*$^{+/-}$ animals. Femoral length was reduced at both 4- and 24-weeks of age in *Axin2*$^{-/-}$ as compared to WT mice (−7% and −5%, respectively), consistent with the decreased limb length previously reported for this mouse model [32] (Supplemental Figure 1). Femoral length was similar between *Runx2*$^{+/-}$ and WT mice at 4 weeks of age, but was reduced (−6%) in 24 week-old *Runx2*$^{+/-}$ animals, consistent with the known role of Runx2 in regulating bone length [33]. Femoral length of the double mutant *Axin2*$^{-/-}$*:Runx2*$^{+/-}$ animals was also reduced as compared to WT mice at both 4 and 24 weeks of age (−7% and −8%, respectively; Supplemental Figure 1). No differences in trabecular bone mass or architecture were noted between any groups at either 4- or 24 weeks of age (Supplemental Table 2).

3.6 Fracture healing is delayed at early stages but accelerated at later stages in double mutant mice

Finally, we examined a model of endochondral bone repair to determine whether the delayed chondrocyte maturation patterns observed in vitro would affect endochondral healing processes in vivo. The healing of transverse, destabilized, double cortical fractures involves successive stages of inflammation, cartilage formation, vascular invasion, osteoblast recruitment, mineralization, and eventually remodeling [29, 34, 35]. *Runx2*$^{+/-}$ and *Axin2*$^{-/-}$*:Runx2*$^{+/-}$ mice demonstrated 25% and a 12% relative increases, respectively, in callus area as compared to WT mice at 21 days post-fracture (Figure 8A). In contrast, callus size was 20 to 21% smaller in *Axin2*$^{-/-}$ as compared to WT mice at days 14 and 21 (−21%) post-fracture. Remnants of Safranin-O staining tissue were observed histologically in the *Axin2*$^{-/-}$*:Runx2*$^{+/-}$ fracture calluses at 21 days post-fracture, but were not observed in other groups (Figure 8B). These data confirm the dominance of Runx2 over Axin2 deficiency in chondrocyte differentiation and early stages of fracture repair and are consistent with observations from the in vitro chondrocyte cultures and frontal sutures. Interestingly, at 28 days post-fracture, double mutant animals diverged from the *Runx2*$^{+/-}$ mice, showing smaller callus size and increased torsional strength. Callus size was 13% smaller in *Axin2*$^{-/-}$*:Runx2*$^{+/-}$ mice as compared to WT mice by day 28 post-fracture. Measurements of torsional strength derived from mechanical testing were more variable, but ultimate torque (a structural property) generally reflected callus size (Figure 8C) as expected [35]. These results indicate more rapid end-stage bone formation in double mutant mice that is on par with that observed in the *Axin2*$^{-/-}$ animals.

4. Discussion

Runx2 and Wnt/β-catenin signaling are essential for bone formation. We recently reported that Runx2 interacts with the Wnt target and negative feedback inhibitor, Axin2, in osteoblasts at a molecular level. Runx2 directly represses transcription of Axin2 mRNA during osteoblast differentiation by binding several regions of the Axin2 promoter, and Runx2-mediated repression of Axin2 transcription depends on histone deacetylase 3 (Hdac3) [18]. *Runx2* haploinsufficiency rescued of several morphological aspects of craniosynostosis phenotype of the *Axin2*$^{-/-}$ single mutants, and gene profiling showed that osteoblasts derived from the bone marrow of *Axin2*$^{-/-}$*:Runx2*$^{+/-}$ mice mimicked temporal osteoblastic gene expression patterns of WT cells, rather than the high osteogenic activity of *Axin2*$^{-/-}$ osteoblasts [18]. While the craniosynostosis-related morphology of *Axin2*$^{-/-}$ skulls was rescued by introducing *Runx2* haploinsufficiency, our previous studies did not address whether Axin2 deficiency would impact the CCD phenotype of *Runx2*$^{+/-}$ mice [18]. Here we investigated the consequences of Axin2 deficiency and resultant high β–catenin levels on bone formation and cleidocranial dysplasia in a *Runx2* haploinsufficient model. Strikingly, Axin2 deficiency did not rescue, but rather exacerbated several aspects of the CCD phenotype of *Runx2*$^{+/-}$ mice, largely due to improper endochondral bone formation. *Axin2*$^{-/-}$*: Runx2*$^{+/-}$ mice had greater calvarial defects as compared to *Runx2*$^{+/-}$ mice in sutures, and primary chondrocytes from these animals demonstrated delayed maturation. Microarray analyses revealed high expression of cartilage-related transcripts and low expression of transcripts related to vasculogenesis in the double mutant animals, supporting a mechanism of improper endochondral bone formation that was later confirmed by histological observation of persistent cartilage in the endocranial layer of the frontal suture. In fracture healing studies, *Axin2*$^{-/-}$*:Runx2*$^{+/-}$ mice had enlarged cartilaginous calluses at the early stages of bone repair. Taken together, these data from three independent models indicate that a full complement of Runx2 is essential for proper chondrocyte development in the early stages of endochondral bone formation in the presence or absence of Axin2 expression, as the positive effects of Axin2-deficiency on chondrocyte hypertrophy could not overcome (and in fact worsened) the impaired chondrocyte development caused by insufficient Runx2 expression. Our data demonstrate a dominant role for Runx2 in chondrocyte maturation, but confirm Axin2 as an important modulator of the terminal stages of endochondral bone formation (Figure 9).

Genetic deletion of Runx2 precludes formation of a mature skeleton [3, 10], and haploinsufficiency impairs calvarial and clavicle development [12]. Several laboratories investigating the CCD phenotype of Runx2-heterozygous mice successfully attenuated the condition. For example, overexpression of Nell-1, a downstream target of Runx2 that promotes of endochondral bone formation, and suppression of Zfp521, an Hdac3 co-factor, each partially rescued the calvarial defects of *Runx2*$^{+/-}$ mice [36, 37]. Similarly, crossing *Runx2* heterozygous mice with mice deficient in Gsk3β, a negative regulator of canonical Wnt signaling, partially rescued the calvarial and clavicle irregularities of *Runx2*$^{+/-}$ single mutant animals [38]. Interestingly, the rescue of the CCD phenotype in this latter model had little to do with elevated β-catenin activity. Rather, Gsk3β deficiency prevented the inhibitory phosphorylation of Runx2 and consequently, increased Runx2 transcriptional

activity of proteins expressed from the remaining allele [38]. Thus, the role of Wnt signaling in the CCD phenotype of *Runx2*$^{+/-}$ mice remained unclear. Our results suggest that Axin2 deficiency and resultant high Wnt signaling may exacerbate the CCD phenotype of *Runx2*$^{+/-}$ mice by delaying endochondral bone formation.

Axin2$^{-/-}$ mice have high canonical Wnt signaling because Axin2 promotes assembly of the β-catenin destruction complex [16, 19, 32]. Wnt/β-catenin signaling stimulates MSC proliferation and osteoblast lineage commitment, but prevents chondrogenic differentiation of MSCs. However, in terminal stages of chondrocyte maturation, temporal induction of β-catenin is required for matrix metalloproteinase expression, and the vascular recruitment stage of endochondral bone formation [39]. Axin2 is an important modulator of this process and inhibits hypertrophy of proliferating chondrocytes [32]. We observed high levels of activated β-catenin staining in the frontal suture of *Axin2*$^{-/-}$ mice, as expected, by both immunohistochemistry and microarray analysis of gene expression. Lower levels of nuclear activated β-catenin were present in the endocranial layer of the frontal suture within *Axin2*$^{-/-}$*:Runx2*$^{+/-}$ mice, specifically in a region with non-ossified wide suture mesenchyme. These data indicate that a full complement of Runx2 is required for Wnt signaling and endochondral bone formation.

The cranial fontanel defect in *Axin2*$^{-/-}$*:Runx2*$^{+/-}$ mice was associated with incomplete formation of the frontal suture. Murine frontal sutures are unique in that they fuse via endochondral mechanisms [19, 30, 40]. Conflicting evidence exists regarding the role of Axin2 and Wnt signaling in the maturation of this suture. It was previously reported that Axin2 levels decrease prior to cartilage formation [19], and that enhanced Wnt signaling promotes fusion of the frontal suture [16]. In contrast, others demonstrated that low levels of Wnt signaling generate the endocranial cartilage template in the frontal suture [41], more consistent with the known role of Wnt signaling in chondrocyte commitment [39]. The reasons for discrepancy between these two models are not yet clear, but differences in genetic backgrounds, suture fusion rates, and anatomical location within the frontal suture are possible explanations [42]. Our data favor the former model, as we observed high Wnt pathway activity and premature fusion of the frontal suture in *Axin2*$^{-/-}$ as compared to WT littermates. Our data also show that Runx2 regulates the terminal stages of frontal suture fusion, as *Axin2*$^{-/-}$*:Runx2*$^{+/-}$ mice exhibit more chondrogenesis but less mineralization in the endocranial layer of the frontal suture. Down-regulation of gene expression related to blood vessel morphogenesis in these mice likely reflects impaired vascularization of this cartilage, leading to defective calvarial formation.

To better address the endochondral bone formation aspect of the *Axin2*$^{-/-}$*: Runx2*$^{+/-}$ mouse phenotype, we first analyzed long bone structure. Femoral length was reduced in both single and double mutant mice, likely reflecting Axin2's role as an inhibitor of differentiating chondrocyte maturation [32] and Runx2's role in modulating chondrocyte proliferation and terminal differentiation [33, 43]. Interestingly, we failed to detect high trabecular bone mass in 24 week-old *Axin2*$^{-/-}$ mice, which conflicts with a previous report on this mouse model [44]. Our conflicting results may be due to experimental differences, including the use of males (as compared to females) in our study, raising questions as to the role of estrogen in the high bone mass phenotype of the *Axin2*$^{-/-}$ animals with age. To exacerbate conditions

of endochondral bone formation for study in the postnatal long bones, we utilized a postnatal fracture repair model. Both *Runx2*$^{+/-}$ and double mutant mice had larger calluses than WT and *Axin2*$^{-/-}$ mice at two weeks post-fracture, confirming the importance of Runx2 in the early stages of endochondral bone formation. However, after four weeks of healing, double mutant animals diverged from the *Runx2*$^{+/-}$ mice, showing smaller callus size and differences in torsional strength indicative of more rapid healing as seen in the *Axin2*$^{-/-}$ mice. Taken together, these data demonstrate a dominant role for Runx2 in chondrocyte differentiation, but confirm Axin2 as an important modulator of the terminal stages of endochondral bone formation.

In conclusion, a mechanistic link exists between Runx2 and Axin2 expression in endochondral bone formation in both the axial and appendicular skeleton. Axin2 is a negative regulator of the Wnt-β-catenin signaling pathway, which is a target for new osteogenic therapies. Furthermore, AXIN2 affects human craniofacial development as AXIN2 mutations are linked to familial tooth agenesis [45, 46]. Interestingly, most humans with CCD feature an opposite phenotype of supernumerary teeth [45-48], providing clinical support for an inverse link between AXIN2 and RUNX2 expression in human skeletal development. Thus, these data shed light on new mechanisms involved in skeletal development and repair by Wnt and Runx2 modulators.

Supplementary Material

Refer to Web version on PubMed Central for supplementary material.

Acknowledgments

The NIH (R01 DE020194, R37 DE012528, T32 AR056950, F32 AR60140, F32 AR061873) and the Mayo Clinic Center for Regenerative Medicine supported this work. MEML, EWB, LRC, AD, SK and JJW contributed to the study design, data acquisition and analysis, and manuscript drafting. MEML, JBL, AJvW, WH, and JJW contributed to the interpretation of data and critical review of the manuscript. MEML and JJW are accountable for the accuracy and integrity of the work. The authors thank Dr. David Razidlo, Xiaodong Li, Bridget Stensgard, and Jim Herrick for technical assistance with animals and histology. The authors also thank the Mayo Clinic Medical Genome Facility Gene Expression Core and Dr. Ying Li from the Mayo Clinic Biomedical Statistics & Informatics Division of Health Sciences Research for microarray data collection and analysis.

REFERENCES

[1]. Kimonis V, Gold JA, Hoffman TL, Panchal J, Boyadjiev SA. Genetics of craniosynostosis. Semin Pediatr Neurol. 2007; 14:150–61. [PubMed: 17980312]

[2]. Mundlos S, Otto F, Mundlos C, Mulliken JB, Aylsworth AS, Albright S, Lindhout D, Cole WG, Henn W, Knoll JH, Owen MJ, Mertelsmann R, Zabel BU, Olsen BR. Mutations involving the transcription factor CBFA1 cause cleidocranial dysplasia. Cell. 1997; 89:773–9. [PubMed: 9182765]

[3]. Otto F, Thornell AP, Crompton T, Denzel A, Gilmour KC, Rosewell IR, Stamp GW, Beddington RS, Mundlos S, Olsen BR, Selby PB, Owen MJ. Cbfa1, a candidate gene for cleidocranial dysplasia syndrome, is essential for osteoblast differentiation and bone development. Cell. 1997; 89:765–71. [PubMed: 9182764]

[4]. Bradley EW, McGee-Lawrence ME, Westendorf JJ. Hdac-mediated control of endochondral and intramembranous ossification. Crit Rev Eukaryot Gene Expr. 2011; 21:101–13. [PubMed: 22077150]

[5]. Monfoulet L, Rabier B, Chassande O, Fricain JC. Drilled hole defects in mouse femur as models of intramembranous cortical and cancellous bone regeneration. Calcified tissue international. 2010; 86:72–81. [PubMed: 19953233]

[6]. Morgan EF, Salisbury Palomares KT, Gleason RE, Bellin DL, Chien KB, Unnikrishnan GU, Leong PL. Correlations between local strains and tissue phenotypes in an experimental model of skeletal healing. Journal of biomechanics. 2010; 43:2418–24. [PubMed: 20546756]

[7]. Alkhiary YM, Gerstenfeld LC, Krall E, Westmore M, Sato M, Mitlak BH, Einhorn TA. Enhancement of experimental fracture-healing by systemic administration of recombinant human parathyroid hormone (PTH 1-34). The Journal of bone and joint surgery. American volume. 2005; 87:731–41. [PubMed: 15805200]

[8]. Kakar S, Einhorn TA, Vora S, Miara LJ, Hon G, Wigner NA, Toben D, Jacobsen KA, Al-Sebaei MO, Song M, Trackman PC, Morgan EF, Gerstenfeld LC, Barnes GL. Enhanced chondrogenesis and Wnt signaling in PTH-treated fractures. J Bone Miner Res. 2007; 22:1903–12. [PubMed: 17680724]

[9]. Huang LF, Fukai N, Selby PB, Olsen BR, Mundlos S. Mouse clavicular development: analysis of wild-type and cleidocranial dysplasia mutant mice. Developmental dynamics: an official publication of the American Association of Anatomists. 1997; 210:33–40. [PubMed: 9286593]

[10]. Komori T, Yagi H, Nomura S, Yamaguchi A, Sasaki K, Deguchi K, Shimizu Y, Bronson RT, Gao YH, Inada M, Sato M, Okamoto R, Kitamura Y, Yoshiki S, Kishimoto T. Targeted disruption of Cbfa1 results in a complete lack of bone formation owing to maturational arrest of osteoblasts. Cell. 1997; 89:755–64. [PubMed: 9182763]

[11]. Takarada T, Hinoi E, Nakazato R, Ochi H, Xu C, Tsuchikane A, Takeda S, Karsenty G, Abe T, Kiyonari H, Yoneda Y. An analysis of skeletal development in osteoblast-specific and chondrocyte-specific runt-related transcription factor-2 (Runx2) knockout mice. Journal of bone and mineral research: the official journal of the American Society for Bone and Mineral Research. 2013; 28:2064–9.

[12]. Lou Y, Javed A, Hussain S, Colby J, Frederick D, Pratap J, Xie R, Gaur T, van Wijnen AJ, Jones SN, Stein GS, Lian JB, Stein JL. A Runx2 threshold for the cleidocranial dysplasia phenotype. Hum Mol Genet. 2009; 18:556–68. [PubMed: 19028669]

[13]. Zheng Q, Sebald E, Zhou G, Chen Y, Wilcox W, Lee B, Krakow D. Dysregulation of chondrogenesis in human cleidocranial dysplasia. Am J Hum Genet. 2005; 77:305–12. [PubMed: 15952089]

[14]. Mefford HC, Shafer N, Antonacci F, Tsai JM, Park SS, Hing AV, Rieder MJ, Smyth MD, Speltz ML, Eichler EE, Cunningham ML. Copy number variation analysis in single-suture craniosynostosis: multiple rare variants including RUNX2 duplication in two cousins with metopic craniosynostosis. Am J Med Genet A. 2010; 152A:2203–10. [PubMed: 20683987]

[15]. Maeno T, Moriishi T, Yoshida CA, Komori H, Kanatani N, Izumi S, Takaoka K, Komori T. Early onset of Runx2 expression caused craniosynostosis, ectopic bone formation, and limb defects. Bone. 2011; 49:673–82. [PubMed: 21807129]

[16]. Liu B, Yu HM, Hsu W. Craniosynostosis caused by Axin2 deficiency is mediated through distinct functions of beta-catenin in proliferation and differentiation. Dev Biol. 2007; 301:298–308. [PubMed: 17113065]

[17]. Yu HM, Jerchow B, Sheu TJ, Liu B, Costantini F, Puzas JE, Birchmeier W, Hsu W. The role of Axin2 in calvarial morphogenesis and craniosynostosis. Development. 2005; 132:1995–2005. [PubMed: 15790973]

[18]. McGee-Lawrence ME, Li X, Bledsoe KL, Wu H, Hawse JR, Subramaniam M, Razidlo DF, Stensgard BA, Stein GS, van Wijnen AJ, Lian JB, Hsu W, Westendorf JJ. Runx2 protein represses Axin2 expression in osteoblasts and is required for craniosynostosis in Axin2-deficient mice. The Journal of biological chemistry. 2013; 288:5291–302. [PubMed: 23300083]

[19]. Maruyama T, Mirando AJ, Deng CX, Hsu W. The balance of WNT and FGF signaling influences mesenchymal stem cell fate during skeletal development. Sci Signal. 2010; 3:ra40. [PubMed: 20501936]

[20]. Schroeder TM, Westendorf JJ. Histone deacetylase inhibitors promote osteoblast maturation. J Bone Miner Res. 2005; 20:2254–63. [PubMed: 16294278]

[21]. Razidlo DF, Whitney TJ, Casper ME, McGee-Lawrence ME, Stensgard BA, Li X, Secreto FJ, Knutson SK, Hiebert SW, Westendorf JJ. Histone deacetylase 3 depletion in osteo/chondroprogenitor cells decreases bone density and increases marrow fat. PLOS One. 2010; 5:e11492. [PubMed: 20628553]

[22]. Pfaffl MW. A new mathematical model for relative quantification in real-time RT-PCR. Nucleic Acids Res. 2001; 29:e45. [PubMed: 11328886]

[23]. Gosset M, Berenbaum F, Thirion S, Jacques C. Primary culture and phenotyping of murine chondrocytes. Nat Protoc. 2008; 3:1253–60. [PubMed: 18714293]

[24]. Bradley EW, Carpio LR, Westendorf JJ. Histone deacetylase 3 suppression increases PH domain and leucine-rich repeat phosphatase (Phlpp)1 expression in chondrocytes to suppress Akt signaling and matrix secretion. The Journal of biological chemistry. 2013; 288:9572–82. [PubMed: 23408427]

[25]. Soung do Y, Dong Y, Wang Y, Zuscik MJ, Schwarz EM, O'Keefe RJ, Drissi H. Runx3/AML2/Cbfa3 regulates early and late chondrocyte differentiation. J Bone Miner Res. 2007; 22:1260–70. [PubMed: 17488194]

[26]. Bradley EW, Drissi MH. Wnt5b regulates mesenchymal cell aggregation and chondrocyte differentiation through the planar cell polarity pathway. J Cell Physiol. 2011; 226:1683–93. [PubMed: 21413026]

[27]. Bradley EW, Drissi MH. WNT5A regulates chondrocyte differentiation through differential use of the CaN/NFAT and IKK/NF-kappaB pathways. Mol Endocrinol. 2010; 24:1581–93. [PubMed: 20573686]

[28]. McGee-Lawrence ME, McCleary-Wheeler AL, Secreto FJ, Razidlo DF, Zhang M, Stensgard BA, Li X, Stein GS, Lian JB, Westendorf JJ. Suberoylanilide hydroxamic acid (SAHA; vorinostat) causes bone loss by inhibiting immature osteoblasts. Bone. 2011; 48:1117–26. [PubMed: 21255693]

[29]. Manigrasso MB, O'Connor JP. Comparison of fracture healing among different inbred mouse strains. Calcified tissue international. 2008; 82:465–74. [PubMed: 18528610]

[30]. Bradley JP, Levine JP, Roth DA, McCarthy JG, Longaker MT. Studies in cranial suture biology: IV. Temporal sequence of posterior frontal cranial suture fusion in the mouse. Plast Reconstr Surg. 1996; 98:1039–45. [PubMed: 8911474]

[31]. Sahar DE, Longaker MT, Quarto N. Sox9 neural crest determinant gene controls patterning and closure of the posterior frontal cranial suture. Dev Biol. 2005; 280:344–61. [PubMed: 15882577]

[32]. Dao DY, Yang X, Flick LM, Chen D, Hilton MJ, O'Keefe RJ. Axin2 regulates chondrocyte maturation and axial skeletal development. J Orthop Res. 2010; 28:89–95. [PubMed: 19623616]

[33]. Zhang S, Xiao Z, Luo J, He N, Mahlios J, Quarles LD. Dose-dependent effects of Runx2 on bone development. Journal of bone and mineral research: the official journal of the American Society for Bone and Mineral Research. 2009; 24:1889–904.

[34]. Jepsen KJ, Price C, Silkman LJ, Nicholls FH, Nasser P, Hu B, Hadi N, Alapatt M, Stapleton SN, Kakar S, Einhorn TA, Gerstenfeld LC. Genetic variation in the patterns of skeletal progenitor cell differentiation and progression during endochondral bone formation affects the rate of fracture healing. Journal of bone and mineral research: the official journal of the American Society for Bone and Mineral Research. 2008; 23:1204–16.

[35]. Morgan EF, Mason ZD, Chien KB, Pfeiffer AJ, Barnes GL, Einhorn TA, Gerstenfeld LC. Micro-computed tomography assessment of fracture healing: relationships among callus structure, composition, and mechanical function. Bone. 2009; 44:335–44. [PubMed: 19013264]

[36]. Zhang X, Ting K, Bessette CM, Culiat CT, Sung SJ, Lee H, Chen F, Shen J, Wang JJ, Kuroda S, Soo C. Nell-1, a key functional mediator of Runx2, partially rescues calvarial defects in Runx2(+/−) mice. J Bone Miner Res. 2011; 26:777–91. [PubMed: 20939017]

[37]. Hesse E, Saito H, Kiviranta R, Correa D, Yamana K, Neff L, Toben D, Duda G, Atfi A, Geoffroy V, Horne WC, Baron R. Zfp521 controls bone mass by HDAC3-dependent attenuation of Runx2 activity. J Cell Biol. 2010; 191:1271–83. [PubMed: 21173110]

[38]. Kugimiya F, Kawaguchi H, Ohba S, Kawamura N, Hirata M, Chikuda H, Azuma Y, Woodgett JR, Nakamura K, Chung UI. GSK-3beta controls osteogenesis through regulating Runx2 activity. PLOS One. 2007; 2:e837. [PubMed: 17786208]

[39]. Day TF, Guo X, Garrett-Beal L, Yang Y. Wnt/beta-catenin signaling in mesenchymal progenitors controls osteoblast and chondrocyte differentiation during vertebrate skeletogenesis. Dev Cell. 2005; 8:739–50. [PubMed: 15866164]

[40]. Sahar DE, Behr B, Fong KD, Longaker MT, Quarto N. Unique modulation of cadherin expression pattern during posterior frontal cranial suture development and closure. Cells, tissues, organs. 2010; 191:401–13. [PubMed: 20051668]

[41]. Behr B, Longaker MT, Quarto N. Differential activation of canonical Wnt signaling determines cranial sutures fate: a novel mechanism for sagittal suture craniosynostosis. Dev Biol. 2010; 344:922–40. [PubMed: 20547147]

[42]. Behr B, Longaker MT, Quarto N. Absence of endochondral ossification and craniosynostosis in posterior frontal cranial sutures of Axin2(−/−) mice. PLOS One. 2013; 8:e70240. [PubMed: 23936395]

[43]. Chen H, Ghori-Javed FY, Rashid H, Adhami MD, Serra R, Gutierrez SE, Javed A. Runx2 Regulates Endochondral Ossification through Control of Chondrocyte Proliferation and Differentiation. Journal of bone and mineral research: the official journal of the American Society for Bone and Mineral Research. 2014

[44]. Yan Y, Tang D, Chen M, Huang J, Xie R, Jonason JH, Tan X, Hou W, Reynolds D, Hsu W, Harris SE, Puzas JE, Awad H, O'Keefe RJ, Boyce BF, Chen D. Axin2 controls bone remodeling through the beta-catenin-BMP signaling pathway in adult mice. J Cell Sci. 2009; 122:3566–78. [PubMed: 19737815]

[45]. Hu JC, Simmer JP. Developmental biology and genetics of dental malformations. Orthod Craniofac Res. 2007; 10:45–52. [PubMed: 17552940]

[46]. Lammi L, Arte S, Somer M, Jarvinen H, Lahermo P, Thesleff I, Pirinen S, Nieminen P. Mutations in AXIN2 cause familial tooth agenesis and predispose to colorectal cancer. Am J Hum Genet. 2004; 74:1043–50. [PubMed: 15042511]

[47]. Suda N, Hattori M, Kosaki K, Banshodani A, Kozai K, Tanimoto K, Moriyama K. Correlation between genotype and supernumerary tooth formation in cleidocranial dysplasia. Orthod Craniofac Res. 2010; 13:197–202. [PubMed: 21040462]

[48]. Suda T, Takahashi N, Martin TJ. Modulation of osteoclast differentiation. Endocr Rev. 1992; 13:66–80. [PubMed: 1555533]

Highlights

- Axin2 deficiency exacerbated the CCD phenotype of Runx2$^{+/-}$ mice.
- Axin2 deficiency delays chondrocyte maturation in Runx2$^{+/-}$ mice.
- Axin2 deficiency delays chondrocyte maturation in vitro and during fracture repair.
- Runx2 has a dominant role in chondrocyte maturation.
- Axin2 modulates terminal stages of endochondral ossification.

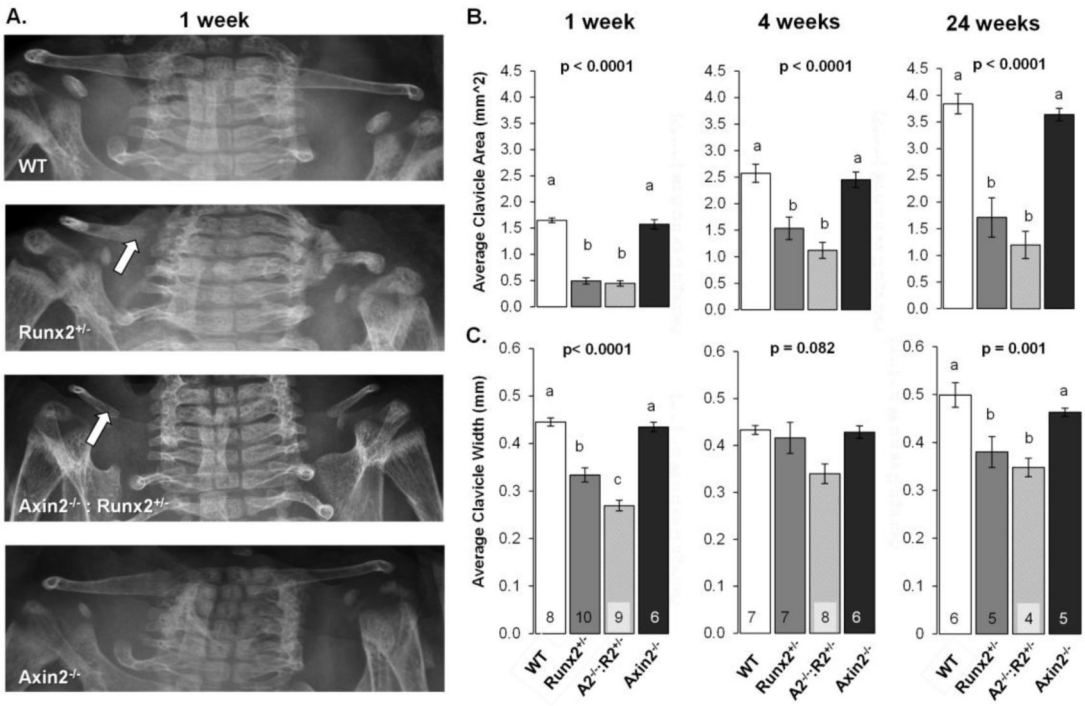

Figure 1.

Axin2 deficiency does not rescue clavicle defects in *Runx2*$^{+/-}$ mice. A) Digital radiographs of 1 week-old mice. Arrows point to medial aspects of the clavicles. B) Average clavicle areas in mice at 1, 4, and 24 weeks of age. C) Average clavicle width of mice at the indicated ages. Bars with different superscript letters are statistically different from one another. The number of samples per group (in panels B and C) is indicated within the bars of panel C.

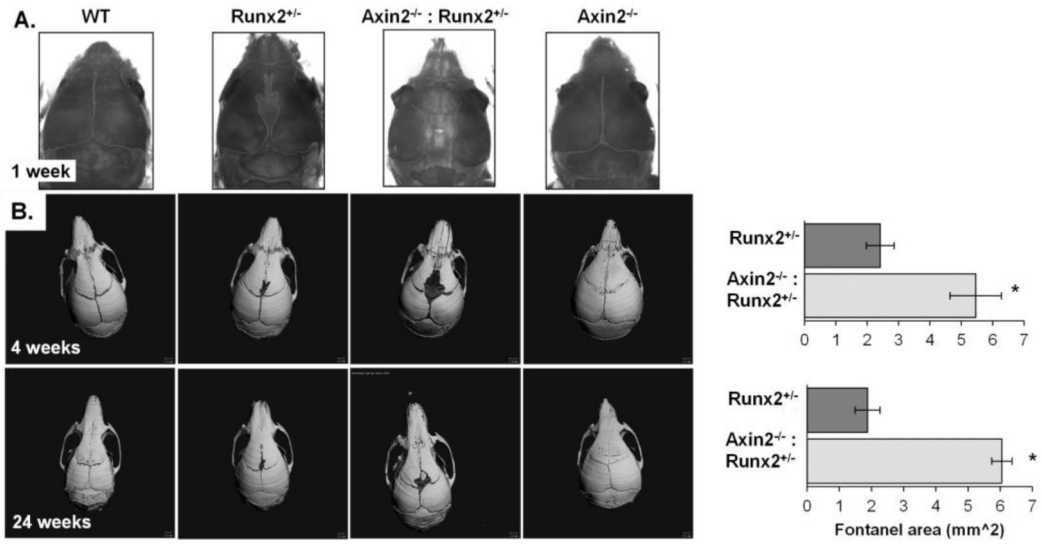

Figure 2.

Axin2 deficiency exacerbates the fontanel defects in *Runx2*$^{+/-}$ mice. A) Whole mount staining of 1 week-old mice. B) Micro-CT reconstructions of skulls from 4 and 24 week-old mice. The number of samples analyzed is indicated in the bars. The WT and *Axin2*$^{-/-}$ mice are not represented in the graph because they do not have open fontanels. *$p < 0.05$ vs. WT mice.

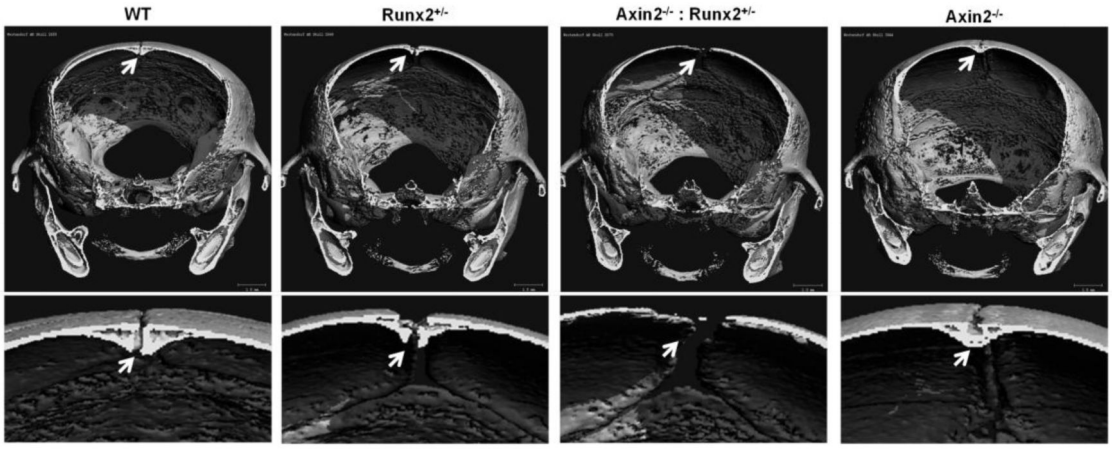

Figure 3.

The endocranial layer of the frontal suture does not mineralize in the *Axin2*$^{-/-}$:*Runx2*$^{+/-}$ mice. Digital sections were collected from micro-CT reconstructions of 4 week-old mice. The endocranial layer of the frontal suture (arrow) is magnified 300x in the lower panel.

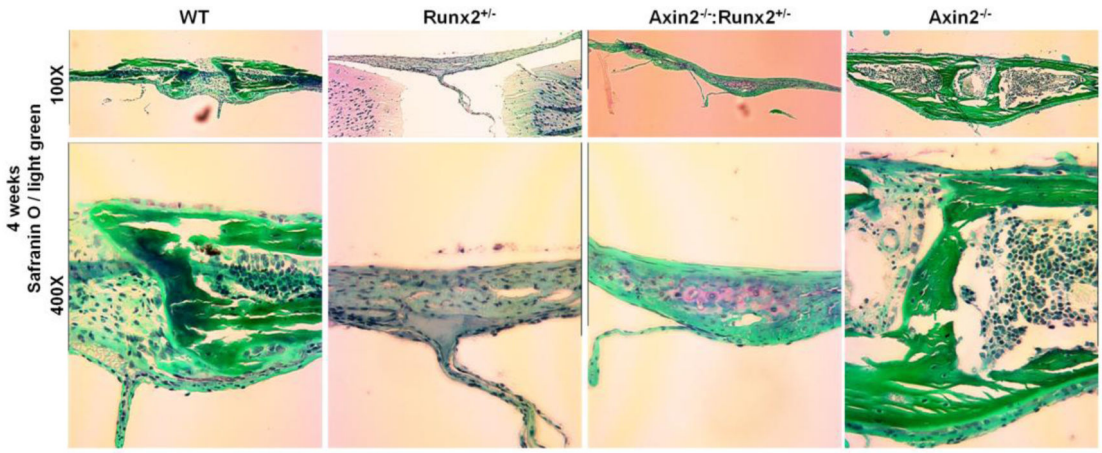

Figure 4.

Cartilage persists in the frontal sutures of *Axin2*$^{-/-}$:*Runx2*$^{+/-}$ mice. Histological analyses of 4 week-old animals were performed with Safranin O and Light Green stains.

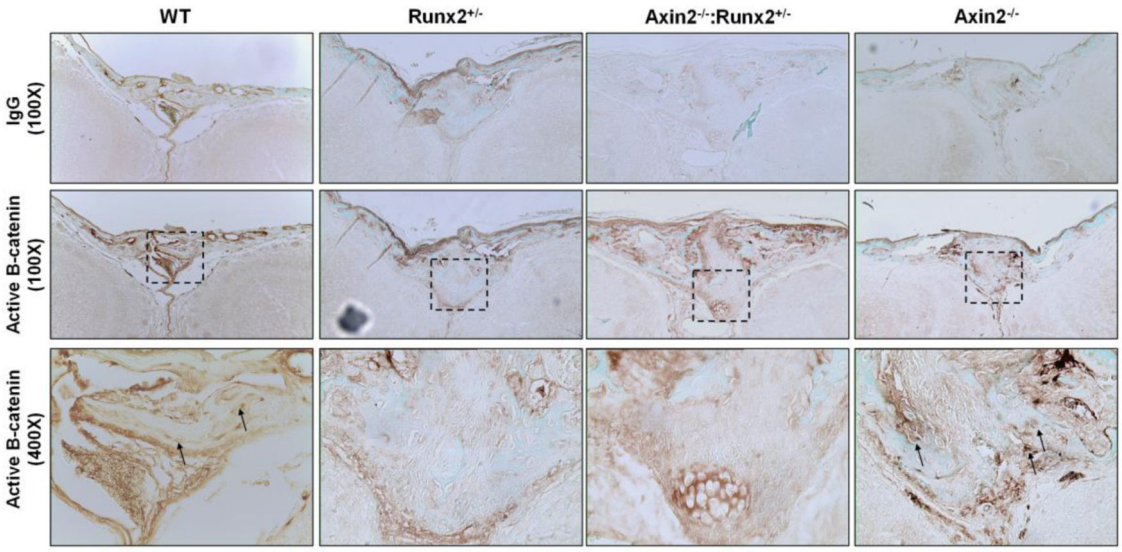

Figure 5.

Frontal sutures of *Axin2*$^{-/-}$*:Runx2*$^{+/-}$ mice lack nuclear staining for active β-catenin. Immunohistochemistry for unphosphorylated (active) β-catenin in the frontal suture of 8 day-old mice demonstrates higher nuclear β-catenin staining in WT and *Axin2*$^{-/-}$ animals. Nuclear beta catenin staining is detectable in the ectocranial layer of the frontal suture of *Axin2*$^{-/-}$*:Runx2*$^{+/-}$ mice, but is not seen in the cell nuclei of the endocranial layer.

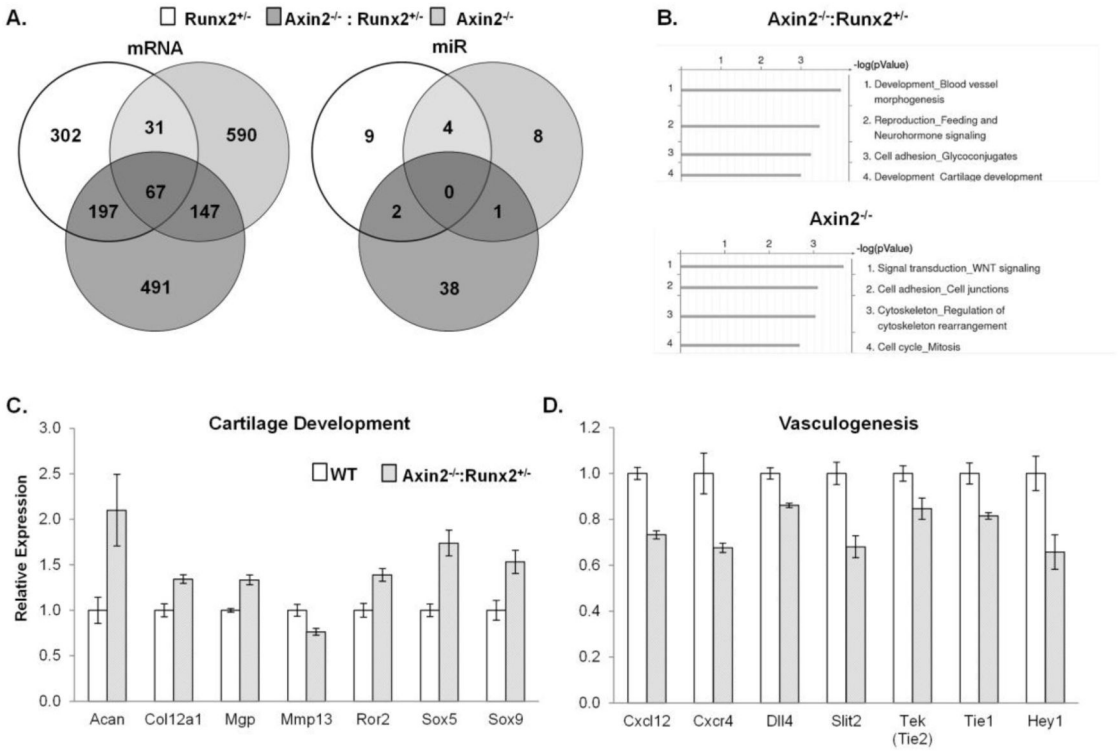

Figure 6.

Chondrogenesis genes are increased while vasculogenesis genes are repressed in *Axin2*$^{-/-}$*:Runx2*$^{+/-}$ mice. A) Venn diagrams of the number of mRNA and miRNA transcripts differentially expressed in calvarial explants of each mutant as compared to WT mice. B) GeneGo process network analysis of differentially expressed genes in *Axin2*$^{-/-}$*:Runx2*$^{+/-}$ mice and *Axin2*$^{-/-}$ mice. C & D) Comparisons of gene expression patterns between *Axin2*$^{-/-}$*:Runx2*$^{+/-}$ and WT mice by qPCR. Means ± SEM of n = 4 mice per group are presented; all genes shown were significantly ($p < 0.05$) differentially expressed in Axin2$^{-/-}$:Runx2$^{+/-}$ as compared to WT mice.

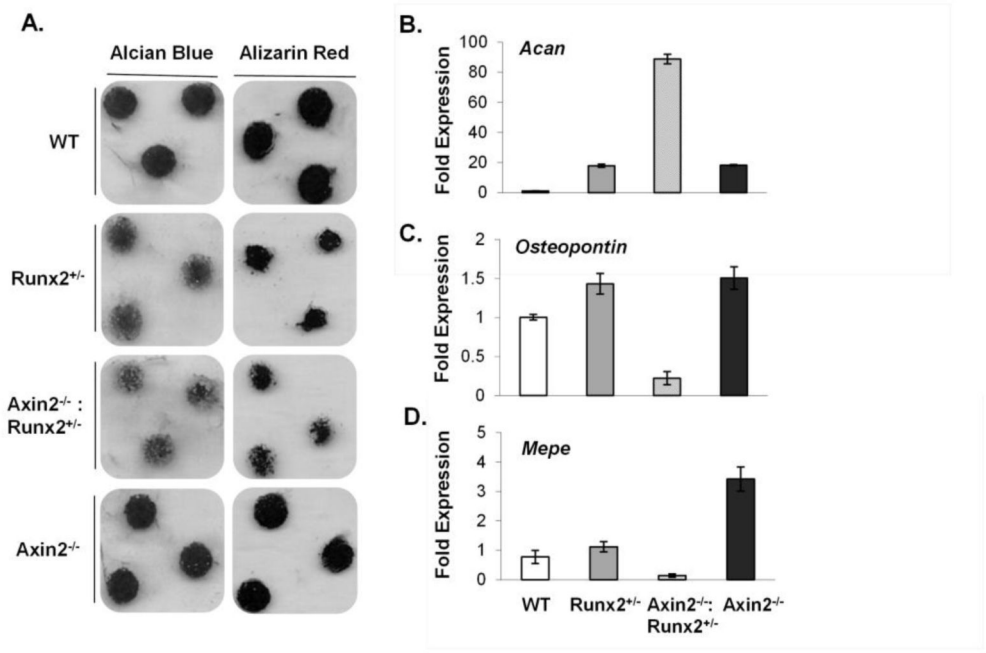

Figure 7.

Axin2 deficiency does not rescue delays in in vitro chondrogenesis cause by Runx2 haploinsufficiency. A) Immature mouse articular chondrocyte micromass cultures were stained with Alcian blue or Alizarin red at day 21. B-D) Relative mRNA levels of Acan, osteopontin, and Mepe in chondrocyte micromass cultures at day 21 were quantified by qPCR.

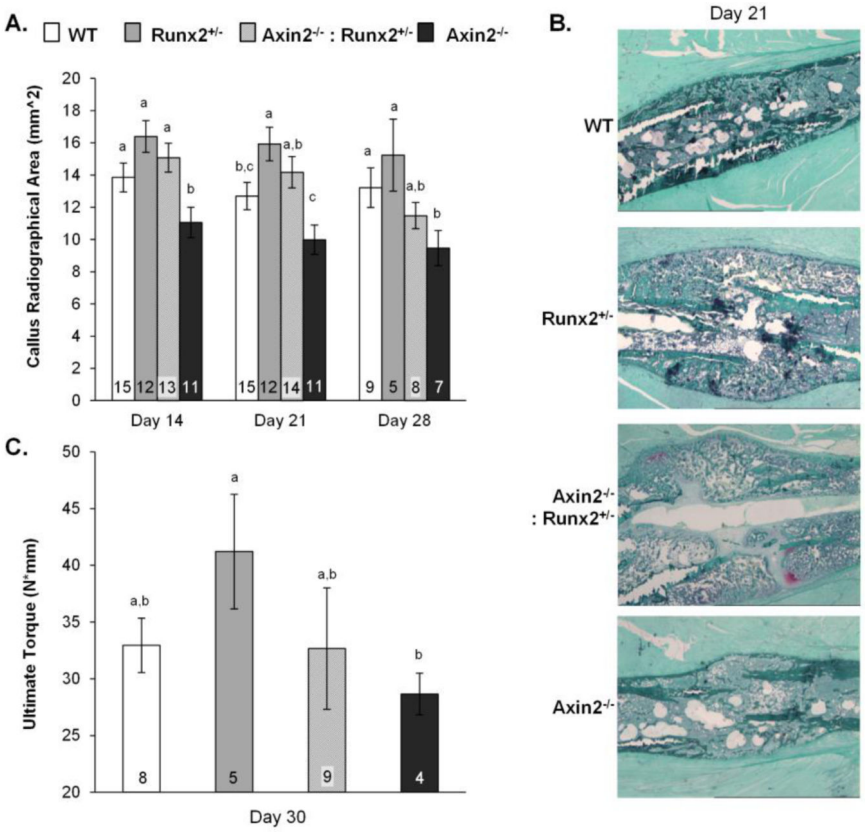

Figure 8.

Fracture healing is delayed at early stages but accelerated at later stages in *Axin2*$^{-/-}$:*Runx2*$^{+/-}$ mice. A) Projected callus areas at 14, 21, and 28 days post-fracture. B) Histological sections of fracture calluses at day 21 post fracture, stained with Safranin O / Light green stains. C) Ultimate torque was quantified by torsional loading to failure on samples harvested on day 30 post-fracture. Bars with different superscript letters are statistically different from one another. The numbers within the bars indicate the sample size of each group.

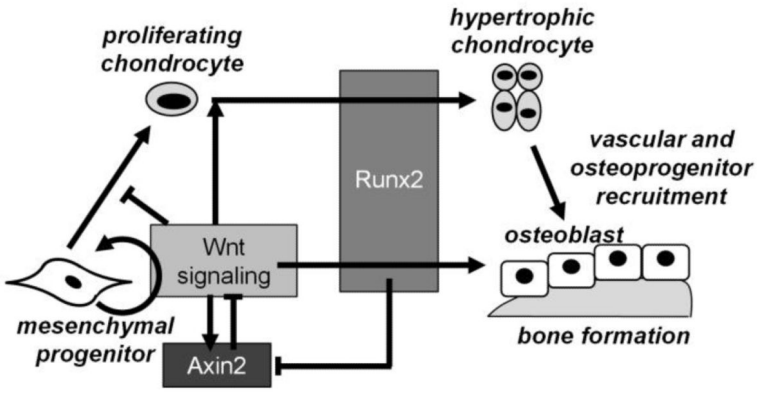

Figure 9.

Molecular interactions between Axin2, Runx2, and Wnt signaling during endochondral and intramembranous bone formation.